CHEMISTRY OF MATERIALS

Article

pubs.acs.org/cm

Spinel Metal Oxide-Alkali Carbonate-Based, Low-Temperature Thermochemical Cycles for Water Splitting and CO_2 Reduction

Bingjun Xu, Yashodhan Bhawe, and Mark E. Davis*

Chemical Engineering, California Institute of Technology, Pasadena, California, 91125, United States

Supporting Information

ABSTRACT: A manganese oxide-based, thermochemical cycle for water splitting below 1000 °C has recently been reported. The cycle involves the shuttling of $Na^{\pm}$ into and out of manganese oxides via the consumption and formation of sodium carbonate, respectively. Here, we explore the combinations of three spinel metal oxides and three alkali carbonates in thermochemical cycles for water splitting and CO_2 reduction. Hydrogen evolution and CO_2 reduction reactions of metal oxides with a given alkali carbonate occur in the following order of decreasing activity: Fe_3O_4 > Mn_3O_4 > Co_3O_4, whereas the reactivity of a given metal oxide with alkali carbonates declines as Li_2CO_3 > Na_2CO_3 > K_2CO_3. While hydrogen evolution and CO_2 reduction reactions occur at a lower temperature on the combinations with the more reactive metal oxide and alkali carbonate, higher thermal reduction temperatures and more difficult alkali ion extractions are observed for the combinations of the more reactive metal oxides and alkali carbonates. Thus, for a thermochemical cycle to be closed at low temperatures, all three reactions of hydrogen evolution (CO_2 reduction), alkali ion extraction, and thermal reduction must proceed within the specified temperature range. Of the systems investigated here, only the Na_2CO_3/Mn_3O_4 combination satisfies these criteria with a maximum operating temperature (850 °C) below 1000 °C.

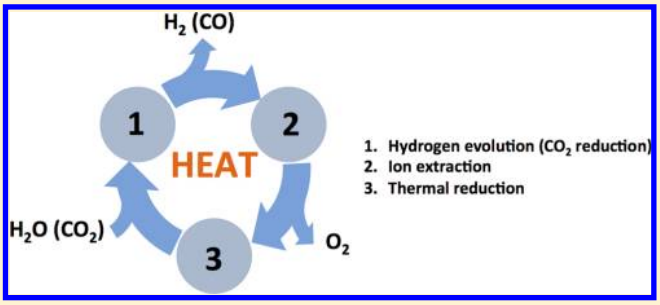

KEYWORDS: *thermochemical cycle, water splitting, CO_2 reduction, spinel metal oxide, alkali carbonate*

INTRODUCTION

There is a considerable amount of under-utilized thermal energy from high-temperature heat sources (>700 °C), for example, nuclear power plants, because the maximum operating temperature for steam turbines is typically below 650 °C (primarily limited by the corrosiveness of high pressure, high temperature steam).[1] Thermochemical cycles for water splitting or CO_2 reduction are able to convert thermal energy into chemical energy stored in hydrogen or CO, respectively. Water (CO_2) is split into stoichiometric amounts of hydrogen (CO) and oxygen in a series of chemical reactions via a closed thermochemical cycle, with heat as the only energy input. No other products are produced in these cycles. There are in general two types of thermochemical cycles: high-temperature, two-step cycles and low-temperature, multistep cycles. The former usually employs relatively simple reactions and benign chemicals, for example, transition metals and metal oxides; however, the operating temperature required to close the cycle is typically higher than 1500 °C.[2−4] Currently, heat sources with such high temperatures, for example, high temperature solar concentrators, are still scarce. In contrast, heat sources at temperature range of 700−1000 °C are much more abundant, for example, nuclear power plants and medium-scale solar concentrators. In addition, high-temperature operating fluids, for example, molten salts,[5] have been developed to work in this temperature range. Low-temperature multistep thermochemical cycles are designed to operate at 700−1000 °C; however, the toxic and corrosive chemicals involved pose significant environmental and engineering challenges. For example, in each reaction of the three-step sulfur−iodine thermochemical cycle for water splitting, with a highest operating temperature of 850 °C, at least one of the following chemicals are involved: H_2SO_4, HI, SO_2, and I_2.[6]

There are two general approaches for developing thermochemical cycles that are able to take advantage of more accessible heat sources: (1) two-step cycles with low operating temperatures; and (2) multistep cycles without employing toxic or corrosive chemicals. The first approach has been proven to be thermodynamically infeasible.[7,8] Recently, we demonstrated the second approach.[7] We showed that a manganese oxide-based, thermochemical cycle for water splitting can be closed at 850 °C without involving any toxic/corrosive chemicals.[7] This manganese oxide-based thermochemical cycle consists of the following three main steps (detailed description of each step can be found elsewhere[7]):

(1) *Hydrogen evolution step*: Mn(II) in Mn_3O_4 is oxidized by water in the presence of Na_2CO_3, producing hydrogen. The spinel Mn_3O_4 is converted to a layered compound, α-$NaMnO_2$,

Received: November 30, 2012
Revised: March 19, 2013

during this step. The hydrogen evolution step proceeds via two sequential reactions:

(1.1) Mn_3O_4 reacts with Na_2CO_3 in the absence of water, forming α-$NaMnO_2$ and MnO (reaction 1). The Mn(III) species is extracted from Mn_3O_4 through the reaction with Na_2CO_3, leaving the Mn(II) species in the form of MnO.

$$Mn_3O_4(s) + Na_2CO_3(s) \rightarrow 2NaMnO_2(s) + MnO(s) + CO_2(g) \quad (1)$$

(1.2.) Mn(II) oxide is oxidized by water in the presence of Na_2CO_3, producing hydrogen and α-$NaMnO_2$ (reaction 2).

$$2MnO(s) + Na_2CO_3(s) + H_2O(g) \rightarrow 2NaMnO_2(s) + H_2(g) + CO_2(g) \quad (2)$$

(2) *Sodium cation extraction step:* The Mn(III) species in α-$NaMnO_2$ cannot be thermally reduced below 1000 °C,[9] whereas the transition from Mn(III) and Mn(IV) oxides to Mn_3O_4 occurs below 850 °C. Therefore, it is critical to remove the sodium cation from the manganese oxide to close the thermochemical cycle below 1000 °C. The sodium cations in α-$NaMnO_2$ can be substituted with protons when it is suspended in water in the presence of CO_2. Water molecules intercalate into the manganese oxide layers, increasing the distance between the layers and mobilizing sodium cations. Protons from carbonic acid, formed via the reaction of CO_2 and water, can exchange with the sodium cations between manganese oxide layers. When CO_2, and in turn protons, are in excess, almost all sodium cations can be removed from the manganese oxide structure. A disproportionation reaction accompanies the ion exchange process:

$$2Mn(III)(s) \rightarrow Mn(IV)(s) + Mn(II)(s) \quad (3)$$

All Mn(IV) and the majority of Mn(III) species are in a proton exchanged birnessite phase. A fraction of the Mn(II) and the remainder of the Mn(III) are in an amorphous Mn_3O_4 phase, whereas the rest of Mn(II) species exists in the form of $MnCO_3$. Since no net oxidation or reduction reaction occurs during the ion exchange process, the average oxidation state of the Mn remains +3.

(3) *Thermal reduction* reaction: When the solid mixture collected after the sodium cation extraction is heated to 850 °C, it restores to the spinel Mn_3O_4 phase (with the release of CO_2 and O_2 in the process), which can be used in the next cycle.

The net reaction of the cycle is the production of stoichiometric amounts of hydrogen and oxygen from water (4), without the formation of any side products.

$$2H_2O(g) \rightarrow 2H_2(g) + O_2(g) \quad (4)$$

The manganese oxide-based thermochemical cycle described above shares two main common features with the Mn/hydroxide cycle:[10,11] (1) both cycles are based on the redox couple of Mn(II)/Mn(III); and (2) the intercalation and removal of sodium cation into and from manganese oxide structure plays an important role in closing the thermochemical cycle.[9,10,12] However, the manganese oxide-based thermochemical cycle described above also has a number of distinctive features: (1) the cycle is closed at 850 °C, which has the potential of utilizing waste heat from abundant heat sources like nuclear power plants. In contrast, the high temperature step of the Mn/hydroxide cycle takes place at ∼1650 °C, and heat sources with such high temperature are relatively scarce. (2) CO_2 significantly facilitates the complete extraction of sodium cation from $NaMnO_2$; while water alone (as used in the Mn/Hydroxide cycle) results in incomplete sodium extraction from $NaMnO_2$ and in turn causes incomplete thermal reduction of Mn(III).[12] (3) Only 1/3 of Mn in the manganese oxide-based thermochemical cycle is active in the redox cycle when operating at 850 °C, since only 1/3 of Mn in Mn_3O_4 is at the oxidation state of +2. However, this cycle can also function with 100% of Mn as the active redox phase, provided suitable heat sources are available (>1650 °C). Therefore, the manganese oxide-based thermochemical cycle described above can take advantage of a much broader range of heat sources. Other thermochemical cycles based on spinel metal oxides and carbonates involve sacrificial Fe_2O_3, and thus are not closed.[13]

In our previous work, only one type of metal oxide (Mn_3O_4) and alkali carbonate (Na_2CO_3) each were explored. The rates of hydrogen evolution and sodium extraction steps depend sensitively on the redox properties of metals in the spinel oxides and faciliness of intercalation of alkali cations. Therefore, here we investigate a variety of combinations of metal oxides with spinel structure (Mn_3O_4, Fe_3O_4, and Co_3O_4) and alkali carbonates (Li_2CO_3, Na_2CO_3, and K_2CO_3) in thermochemical cycles for both water splitting and CO_2 reduction. The reactivity patterns of the metal oxide and alkali carbonate combinations toward water splitting and CO_2 reduction are elucidated. Guiding principles for developing and optimizing low-temperature thermochemical cycles for water splitting and CO_2 reduction are discussed.

■ EXPERIMENTAL SECTION

Materials Preparation. Fe_3O_4 (95%), Mn_3O_4 (97%), Co_3O_4 (99.5%), Li_2CO_3 (99%), Na_2CO_3 (99.5%), and K_2CO_3 (99%) were purchased from Aldrich and used without further treatment. $Na_2{}^{13}CO_3$ (99% ^{13}C) was purchased from Cambridge Isotope Laboratories and used without further treatment. The mixture of metal oxide (Fe_3O_4, Mn_3O_4, or Co_3O_4) and alkali carbonate (Li_2CO_3, Na_2CO_3, or K_2CO_3) with a molar ratio of 2:3 for the hydrogen evolution step was prepared by mixing these two powders in an agate mortar under ambient conditions. The alkali metal ions were extracted from the respective alkali metal oxides by bubbling CO_2 (99.997%, 10 cc/min) through an aqueous suspension of the powder (∼5 wt % of solid) for 3 h at 80 °C. The powder used for the oxygen evolution step was obtained by separating the solid by centrifugation and drying at 100 °C in air.

Reaction Tests. All reaction tests were conducted in an Altamira Instruments AMI-200 catalyst characterization system equipped with a Dycor Dymaxion 2000 online mass spectrometer. The powders were pelletized, crushed, and sieved, and the particles between 20 and 35 mesh were used for testing. To prevent the alkali metal ions from reacting with the quartz used in the reactor tubes, the particles were supported between layers of 16-mesh alumina sand inside an alumina sheath. Under typical flow conditions, the flow rate of the gas was 50 cc/min. Depending on the experiments, the gases used were Ar (99.999%), CO_2/Ar (2%/98%), or D_2O/Ar (5%/95%). Water (D_2O) vapor was introduced by flowing the carrier gas through a bubbler (50 cc/min) with D_2O at room temperature. D_2O was used instead of H_2O to obtain a better signal-to-noise ratio of the signal in the hydrogen evolution step (m/z = 4 for D_2 instead of m/z = 2 for H_2). A ramp-and-hold temperature profile was used in the characterization of these materials. The typical ramp rate was 20 °C/min, and the hold temperatures were varied as needed. All reactions in this subsection were carried out in the solid−gas phase.

The conditions for water pulse experiments were similar to the flow reactions described above, apart from pulse introduction of D_2O to the gas stream for 2−15 min at the desired sample temperature. The reduction of the ion-extracted oxides was carried out under a 50 cc/min

flow of Ar with a temperature ramp from room temperature to 850–1150 °C at 20 °C/min.

Characterization. Powder X-ray diffraction patterns were collected on a Rigaku Miniflex II diffractometer using Cu Kα radiation.

RESULTS

Mn_3O_4 and Alkali Carbonates (Li_2CO_3, Na_2CO_3 and K_2CO_3). Mn_3O_4 reacts with Li_2CO_3 or Na_2CO_3 in Ar at or below 850 °C, releasing CO_2 as the only product in the gas phase; whereas no appreciable reaction occurs between Mn_3O_4 and K_2CO_3 in this temperature range (Figure 1a, the molar ratio of

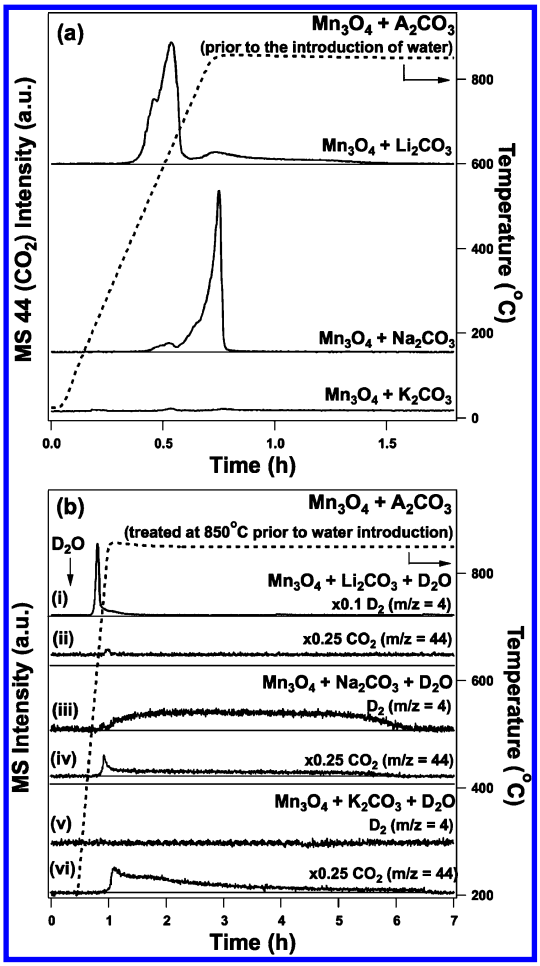

Figure 1. (a) Reaction of Mn_3O_4 with Li_2CO_3 (top trace), Na_2CO_3 (middle trace), and K_2CO_3 (bottom trace) in the absence of water. (b) Solids after the thermal treatment at 850 °C in (a) were cooled down to 200 °C, before D_2O was introduced. The samples were then subjected to a temperature ramp-and-hold treatment to 850 °C in D_2O/Ar (5%/95%). (i, ii) D_2 and CO_2 traces for Mn_3O_4/Li_2CO_3; (iii, iv) D_2 and CO_2 traces for Mn_3O_4/Na_2CO_3; and (v, vi) D_2 and CO_2 traces for Mn_3O_4/K_2CO_3.

Mn_3O_4 and alkali carbonates is 2:3). The CO_2 evolution peaks are at 625 and 850 °C for Mn_3O_4/Li_2CO_3 and Mn_3O_4/Na_2CO_3, respectively. In contrast, no detectable amount of CO_2 is produced with the Mn_3O_4/K_2CO_3 mixture below or at 850 °C. These observations clearly indicate the reactivity of alkali carbonates with Mn_3O_4, gauged by the temperature of CO_2 evolution peak, follows the sequence: Li_2CO_3 > Na_2CO_3 > K_2CO_3.

Unlike the reaction between Mn_3O_4 and Na_2CO_3 (reaction 1), where all Mn(II) species exist in the form of MnO after reaction,[7] $Li_2Mn_2O_4$ and $Li_{0.4}Mn_{0.6}O$ phases are identified by powder X-ray diffraction (XRD) measurements after the temperature ramp-and-hold to 850 °C for Li_2CO_3/Mn_3O_4 in the absence of water (bottom trace, Figure 2a). Since the atomic molar ratio of Li to

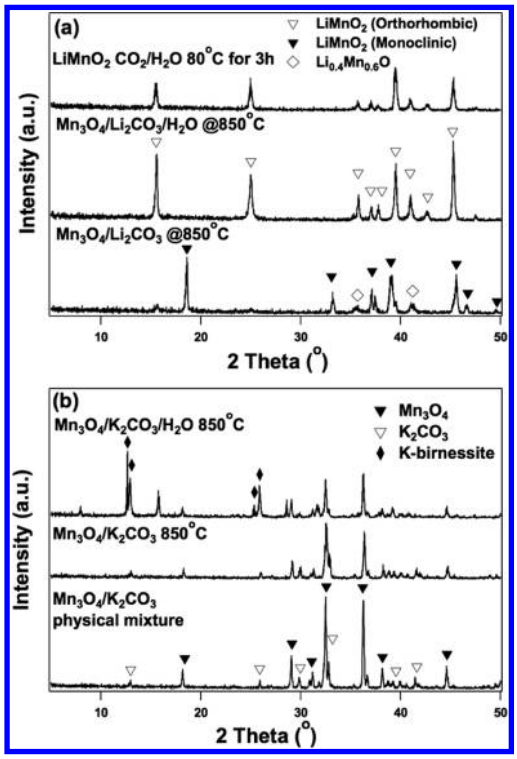

Figure 2. Powder XRD patterns identify intermediate phases in reaction of Mn_3O_4 with alkali carbonates (molar ratio 2:3) under various conditions. (a) Mixture of Mn_3O_4 and Li_2CO_3 heated to 850 °C before (bottom trace) and after (middle trace) the introduction of water. The top trace shows the diffraction pattern of the solid recovered after hydrolyzing $LiMnO_2$ in an aqueous suspension at 80 °C with CO_2 bubbling through for 3 h. (b) Physical mixture of Mn_3O_4 and K_2CO_3 at room temperature (bottom trace) and heated to 850 °C prior to (middle trace) and after (top trace) the introduction of water.

Mn is 1:1 in the starting mixture, a small fraction of Li-containing phase must not be detected by XRD. This result could either be due to the crystal size of the Li-containing phase being below the detection limit of XRD, or due to the Li-containing phase being amorphous. No significant difference in the powder XRD pattern is observed after heating the K_2CO_3/Mn_3O_4 mixture in Ar atmosphere to 850 °C (bottom and middle traces, Figure 2b), consistent with the lack of CO_2 evolution.

Hydrogen evolution is observed for Mn_3O_4/Li_2CO_3 and Mn_3O_4/Na_2CO_3 at or below 850 °C, but not for Mn_3O_4/K_2CO_3 (Figure 1b). The solid after the thermal treatment described in Figure 1a was cooled down to 200 °C, and subjected to a second temperature ramp-and-hold treatment to 850 °C in D_2O/Ar (5%/95%). D_2 evolution is detected from ~540 °C and peaks at ~645 °C and for Mn_3O_4/Li_2CO_3 (trace i in Figure 1b). Little CO_2 is produced during reaction (trace ii in Figure 1b), indicating most of the Li_2CO_3 has reacted with Mn_3O_4 during thermal treatment prior to water introduction. Based on the XRD data, only the orthorhombic $LiMnO_2$ phase is present after the hydrogen evolution reaction, suggesting all Mn(II) in Mn_3O_4 has been oxidized to Mn(III) (middle trace in Figure 2a). D_2 evolution occurs at 850 °C on Mn_3O_4/Na_2CO_3 (trace iii in Figure 1b), and the maximum rate of hydrogen evolution at 850

°C is only 1/50 of that for Mn_3O_4/Li_2CO_3 (an indication that Li_2CO_3 is more active in promoting the hydrogen evolution reaction than Na_2CO_3). For both Mn_3O_4/Li_2CO_3 and Mn_3O_4/Na_2CO_3, the total amounts of hydrogen detected are close to the theoretical amount expected for the total oxidation of the Mn(II) to Mn(III). The concurrent evolution of CO_2 with hydrogen suggests that not all the Na_2CO_3 is consumed in the reaction with Mn_3O_4 prior to the water introduction, and this result is consistent with our previous study.[7] In addition, the fact that the ratio of the amount of CO_2 produced before and after water introduction is very close to 2 indicates that Na_2CO_3 extracts all Mn(III) in Mn_3O_4 but is unable to react with the Mn(II) species in the absence of water.[7] α-$NaMnO_2$ is formed as the only solid product after the hydrogen evolution reaction.[7] No detectable amount of hydrogen is produced for Mn_3O_4/K_2CO_3, suggesting no oxidation of Mn(II) has taken place. CO_2 is observed at 850 °C in the presence of water, and its amount is roughly equal to that expected from the total decomposition of K_2CO_3. Unreacted Mn_3O_4 and K-birnessite are identified after reacting with water at 850 °C by XRD. However, not all peaks in the XRD pattern are accounted for, partly because of the hydroscopic nature of the powder, which forms a wet layer during the time for one powder XRD measurement (~20 min). The solid-phase reaction between Mn_3O_4 with alkali carbonate was carried out prior to the introduction of water to independently determine the temperatures at which these reactions take place. In practical implementations, these two steps can be combined into one.

Li cation removal from $LiMnO_2$ cannot be achieved under similar conditions to that of sodium cation removal from α-$NaMnO_2$, that is, stirring in an aqueous suspension at 80 °C with CO_2 bubbling through for 3 h (henceforth referred to as water/CO_2 treatment). We showed in our previous work that Na cation could be completely extracted from α-$NaMnO_2$ via the water/CO_2 treatment. The XRD patterns of $LiMnO_2$ before and after the water/CO_2 treatment are very similar (top and middle traces, Figure 2a), suggesting that little Li cation has been removed from $LiMnO_2$. Moreover, no detectable amount of O_2 was observed when the water/CO_2 treated $LiMnO_2$ was subjected to a temperature ramp-and-hold procedure to 850 °C in Ar (confirms the lack of Li cation removal during the water/CO_2 treatment).

A fraction of CO_2 formed from the reaction of Mn_3O_4 with Li_2CO_3 is reduced to CO during the temperature ramp-and-hold to 850 °C in the absence of water, but not for Na_2CO_3 or K_2CO_3. For both Mn_3O_4/Li_2CO_3 and Mn_3O_4/Na_2CO_3, all Mn(II) species in Mn_3O_4 are oxidized to Mn(III) in $LiMnO_2$ and α-$NaMnO_2$, respectively, after reacting with water at 850 °C (Figure 1b). The amount of D_2 produced from Mn_3O_4/Na_2CO_3 is within experimental error (±10%) of the theoretical maximum amount; whereas only ~70% of the stoichiometric amount of D_2 was detected for Mn_3O_4/Li_2CO_3. Quantitative mass spectrometric analysis shows that the remaining ~30% of Mn(II) is oxidized by the CO_2 released during the reaction between Mn_3O_4 and Li_2CO_3 prior to the introduction of water, producing CO (Figure 3). In addition to the parent ion of CO_2 (m/z 44), m/z 28 signal is detected as a cracking fragment of CO_2. For pure CO_2, the m/z 28 signal should theoretically trace the parent ion (m/z 44) signal, differing only by a scaling factor.[14] Figure 3 shows that m/z 28 traces exactly m/z 44 by a factor of ~0.2 at temperatures below 685 °C, beyond which the two traces deviate significantly from each other. The difference in the two traces at temperature above 685 °C is attributed to CO produced from the reaction of CO_2 with the Mn(II) species .

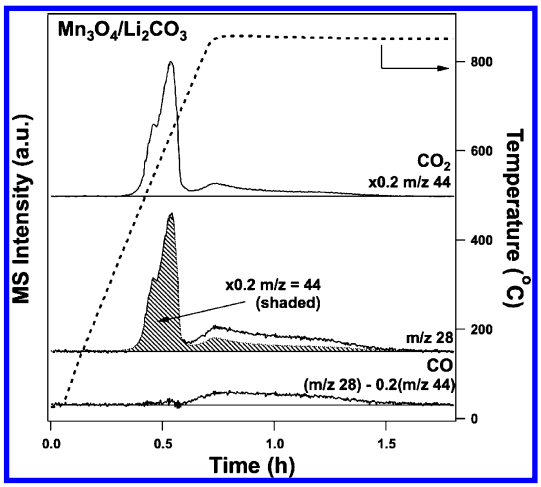

Figure 3. Mass fragmentation analysis shows CO_2 is reduced to CO when reacting with Mn_3O_4 and Li_2CO_3.

Fe_3O_4 and Alkali Carbonates (Li_2CO_3, Na_2CO_3, and K_2CO_3). Both hydrogen evolution and CO_2 reduction reactions occur on Fe_3O_4/Na_2CO_3 at or below 850 °C (Figure 4).

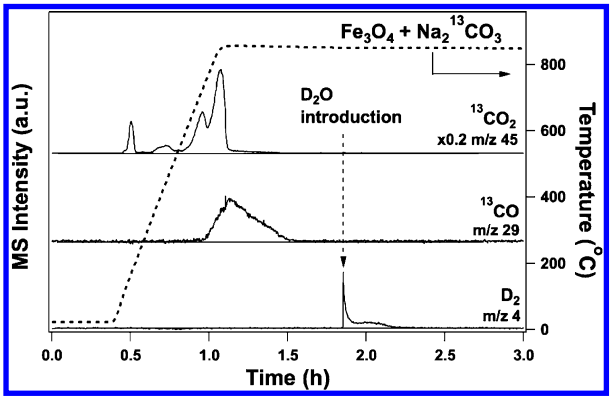

Figure 4. Reaction of Fe_3O_4 with $Na_2{}^{13}CO_3$ confirms reduction of $^{13}CO_2$ to ^{13}CO prior to the introduction of water.

$Na_2{}^{13}CO_3$, rather than $Na_2{}^{12}CO_3$, was used to differentiate the contribution of CO produced from the carbonate and the CO_2 in the feed. Three $^{13}CO_2$ evolution peaks are observed during the temperature ramp-and-hold to 850 °C for $Fe_3O_4/Na_2{}^{13}CO_3$ (molar ratio of 2:3) in Ar. The peak at 165 °C is likely from the decomposition of a sodium bicarbonate impurity in the sodium carbonate, whereas the two main $^{13}CO_2$ evolution peaks at 725 and 850 °C are attributed to the reaction of Fe_3O_4 with $Na_2{}^{13}CO_3$. MS signal for ^{13}CO (m/z 29, corrected for the contribution from the cracking fragment of $^{13}CO_2$) starts to rise at 735 °C, and peaks at 850 °C before returning to the baseline. When D_2O is introduced at 850 °C, a sharp D_2 evolution peak is observed, indicating not all Fe(II) in Fe_3O_4 has been oxidized by CO_2. Approximately 85% and 15% of Fe(II) is oxidized by $^{13}CO_2$ and D_2O, respectively. Replacing $Na_2{}^{13}CO_3$ with $Na_2{}^{12}CO_3$ in the initial solid mixture yielded very similar results. Since the molar ratio of the starting mixture of Fe_3O_4/Na_2CO_3 is 2:3, the total amount of CO_2 released from Na_2CO_3 is 3 times that needed to fully oxidize all the Fe(II) in Fe_3O_4. The fact that ~85% of Fe(II) is oxidized indicates that close to 30% CO_2 is consumed in reduction reaction. Approximately 80% of the Fe(II) is oxidized by CO_2 (produced from the reaction between Fe_3O_4 and Na_2CO_3) during the temperature ramp-and-hold to

dx.doi.org/10.1021/cm3038747 | Chem. Mater. XXXX, XXX, XXX−XXX

750 °C in Ar. The onset of CO evolution occurs at ~735 °C (Figure 4), whereas water oxidizes Fe(II) to Fe(III) with the stoichiometric production of hydrogen at as low as 560 °C (Table 1). The remaining Fe(II) after the completion of CO_2 evolution from the decomposition of carbonates can then be oxidized to Fe(III) by water via hydrogen evolution reaction. Therefore, the temperature of thermal treatment of Fe_3O_4/Na_2CO_3 can be used to control the dominant oxidant for the oxidation of Fe(II) (Figure 5).

Table 1. Onset Temperatures for Hydrogen Evolution and CO_2 Reduction Reactions

sample	onset temperature (°C)		
	CO_2	D_2	CO
Mn_3O_4/Li_2CO_3	400	540	685
Mn_3O_4/Na_2CO_3	515	850	–
Mn_3O_4/K_2CO_3	–	–	–
Fe_3O_4/Li_2CO_3	375	510	675
Fe_3O_4/Na_2CO_3	385	500	735
Fe_3O_4/K_2CO_3	445	500	805

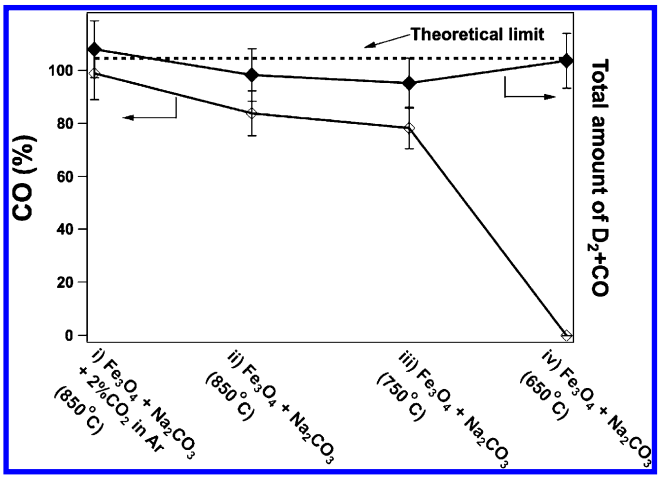

Figure 5. Percentage of CO of the reduction products (H_2 and CO) and total amount of H_2 and CO formed when the physical mixture of Fe_3O_4/Na_2CO_3 (molar ratio 2:3) reacts (i) at 850 °C with 2% CO_2 in the carrier gas (Ar); (ii) at 850 °C in Ar; (iii) at 750 °C in Ar; and (iv) at 650 °C in Ar. D_2O was introduced after the completion of CO_2 evolution from the decomposition of Na_2CO_3 to oxidize the remaining Fe(II) species to Fe(III). The dashed line shows the theoretical maximum amount of H_2 and CO can be formed per mole of Mn.

All the Fe(II) is oxidized to Fe(III) by CO_2 during the temperature ramp-and-hold to 850 °C in CO_2/Ar (2%/98%) (Figure 5), producing a stoichiometric amount of CO with respect to Fe(II). This result suggests that the incomplete oxidation of Fe(II) during the temperature ramp-and-hold procedure conducted in Ar is caused by the limited supply of CO_2. This speculation is also supported by the observation that the MS signals for ^{13}CO and $^{13}CO_2$ decrease simultaneously (Figure 4). To deconvolute the contributions of the CO_2 that evolves from the decomposition of the Na_2CO_3 and the CO_2 in the carrier gas in the CO_2 reduction reaction, $Fe_3O_4/Na_2{}^{13}CO_3$ was subjected to a temperature ramp-and-hold to 850 °C in a $^{12}CO_2$/Ar (2%/98%) atmosphere (Figure 6). The onset of the ^{13}CO and ^{12}CO peaks occurs at similar temperature (~735 °C). The majority of the reduction product initially is ^{13}CO,

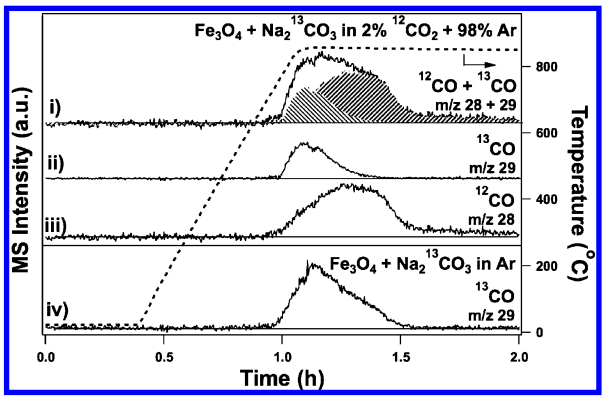

Figure 6. CO_2 reduction with $Fe_3O_4/Na_2{}^{13}CO_3$ in the presence ((i), (ii), and (iii)) and absence (iv) of $^{12}CO_2$ in the feed.

suggesting $^{13}CO_2$ from $Na_2{}^{13}CO_3$ is preferentially reduced. The proximity of the newly formed $^{13}CO_2$ to the Fe(II) species plays a key role. ^{12}CO becomes the dominant reduction product after $^{13}CO_2$ is exhausted. ^{13}CO accounts for approximately 30% of the reduction product, and the remainder is ^{12}CO, with the total amount of CO produced (^{12}CO and ^{13}CO) being close to the amount required to fully oxidize all Fe(II) to Fe(III) (within ±10%).

Hydrogen evolution or CO_2 reduction reaction pathways can be controlled reversibly by tuning the relative concentrations of CO_2 and water. Upon the introduction of the first D_2O pulse to Fe_3O_4/Na_2CO_3 at 850 °C, the rate of CO production instantaneously decreases by more than a factor of 10, and D_2 evolution is observed (Figure 7). In addition, the CO_2 concentration also spikes upon D_2O introduction, indicating less CO_2 is consumed in the reduction reaction. The reverse occurs when the D_2O pulse stops, that is, CO production recovers instantaneously and the D_2 signal decreases to baseline. The pathway for oxidizing Fe(II) to Fe(III) can be controlled by the relative amounts of CO_2 and water present until the Fe(II) species is exhausted.

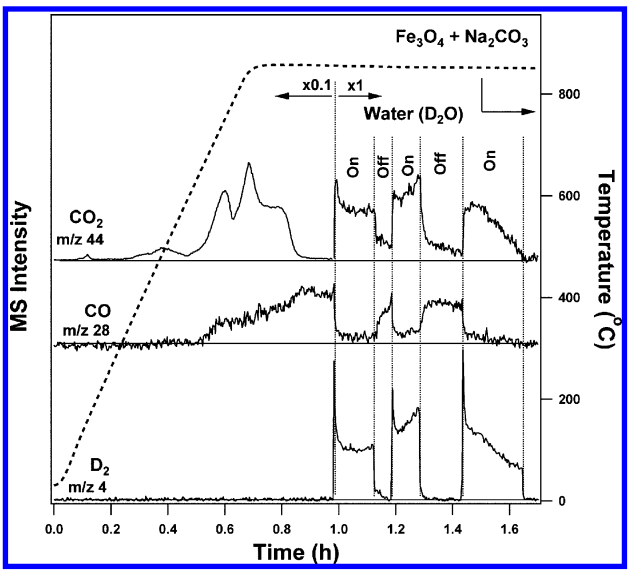

Figure 7. Water pulse experiments show the relative concentration of CO_2 and water controls the contribution of hydrogen evolution and CO_2 reduction over Fe_3O_4 and Na_2CO_3.

dx.doi.org/10.1021/cm3038747 | Chem. Mater. XXXX, XXX, XXX−XXX

CO_2 reduction and hydrogen evolution reactions also take place on Fe_3O_4/Li_2CO_3 and Fe_3O_4/K_2CO_3 (Figure 8). The CO

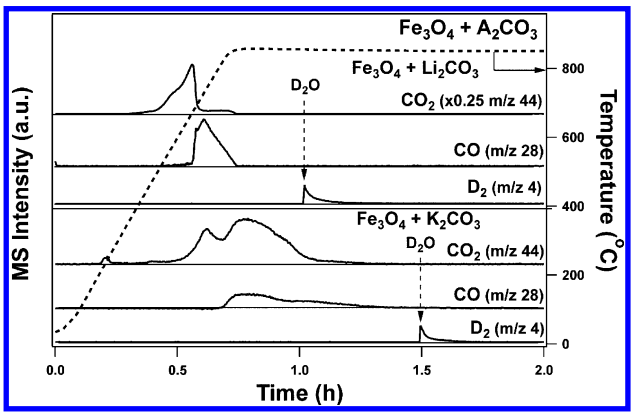

Figure 8. Reactions of Fe_3O_4 with Li_2CO_3 and K_2CO_3 show both CO_2 reduction and hydrogen evolution.

evolution during the temperature ramp-and-hold to 850 °C in Ar starts at 680 and 815 °C for Fe_3O_4/Li_2CO_3 and Fe_3O_4/K_2CO_3, respectively. Water (D_2O) was introduced at 850 °C after the CO signal returns to baseline, and the amounts of D_2 produced account for approximately 20% and 10% of the Fe(II) in Fe_3O_4/Li_2CO_3 and Fe_3O_4/K_2CO_3 respectively. The temperatures for the onset of the D_2 evolution for Fe_3O_4 and carbonates during the temperature ramp-and-hold in D_2O/Ar (5%/95%) are all around 500 °C (Supporting Information, Figure S1).

The powder XRD patterns show only the $AFeO_2$ (A = Li, Na, and K) phases after the temperature ramp-and-hold to 850 °C in Ar (Figure 9). These results are consistent with the observation

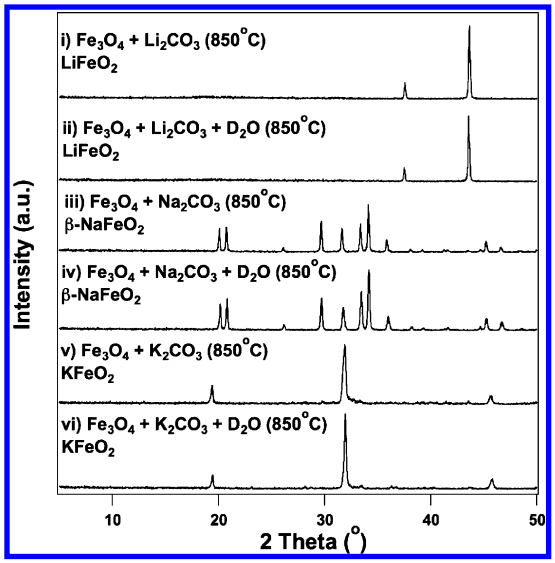

Figure 9. XRD patterns of solids collected after reacting the physical mixture of Fe_3O_4 and alkali carbonates in the absence and presence of D_2O at 850 °C.

that 80% or more of the Fe(II) in Fe_3O_4 is oxidized to Fe(III) by the CO_2 from the carbonates. No detectable change was observed for the solids collected before and after the introduction of water at 850 °C for all Fe_3O_4 and alkali carbonate systems.

Sodium and potassium can be removed from the iron oxide structure via the water/CO_2 treatment, resulting in a hydrated Fe(III) phase, whereas Li cation removal from $LiFeO_2$ cannot be achieved under similar conditions.

Co_3O_4 and Alkali Carbonates (Li_2CO_3, Na_2CO_3, and K_2CO_3). No CO_2 reduction was observed during the temperature ramp-and-hold to 850 °C for Co_3O_4 with all three alkali carbonates (Li_2CO_3, Na_2CO_3, and K_2CO_3) in Ar; nor did hydrogen evolution occur upon the introduction of D_2O at 850 °C. However, Co_3O_4 does react with Li_2CO_3 during the temperature ramp to 850 °C, as evidenced by the $LiCoO_2$ and $Li_{0.21}Co_{0.79}O$ phases identified by powder XRD measurement of the solid collected after the thermal treatment (Figure 10) and

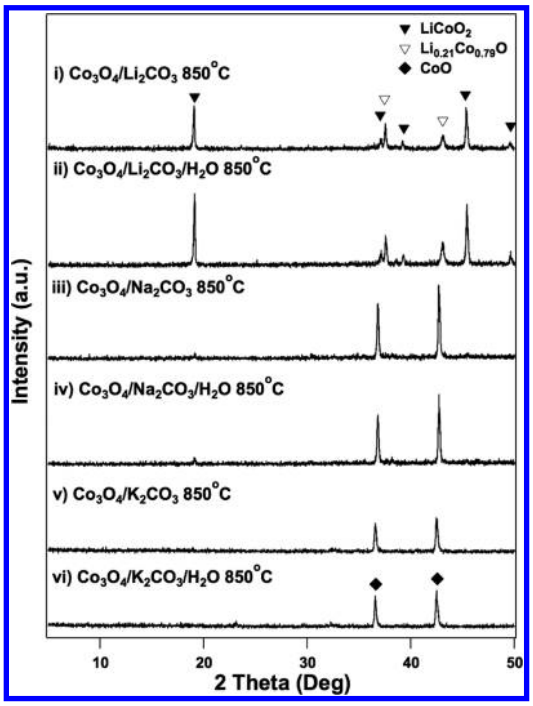

Figure 10. Powder XRD patterns of the solid collected after reacting Co_3O_4 with Li_2CO_3, Na_2CO_3, and K_2CO_3 at 850 °C in the absence ((i), (iii), and (v), respectively) and presence ((ii), (iv), and (vi), respectively) of water.

the sharp CO_2 evolution peak at 575 °C (Figure 11). A CO_2 evolution peak occurs at ~850 °C and has a long tail for both Co_3O_4/Na_2CO_3 and Co_3O_4/K_2CO_3 mixtures during the temperature ramp-and-hold procedure. The total amount of CO_2 evolved is close to that expected for total decomposition of Na_2CO_3 and K_2CO_3. No sodium or potassium-containing phase is identified by XRD after the temperature and hold procedure for Co_3O_4/Na_2CO_3 and Co_3O_4/K_2CO_3, also suggesting the total decomposition of the carbonates. The lack of crystalline sodium or potassium containing phases might be attributed to the hydroscopic nature of sodium and potassium oxides and hydroxides. The XRD patterns show little change after the introduction of water at 850 °C for all alkali carbonates, consistent with the lack of hydrogen evolution.

Thermal Reduction of the Metal Oxides. After removing alkali cation from the metal oxide structure, the solids are subject to temperature ramp-and-hold procedures in Ar to thermally reduce to the spinel oxides (Figure 12). The alkali cation extracted Mn(III) and Fe(III) oxides are fully reduced to Mn_3O_4 and Fe_3O_4 at 850 and 1150 °C, respectively, similar to the temperatures for thermal reduction of Mn_2O_3 and Fe_2O_3. Co_3O_4 is reduced to CoO during the temperature ramp of the Co_3O_4/

dx.doi.org/10.1021/cm3038747 | Chem. Mater. XXXX, XXX, XXX−XXX

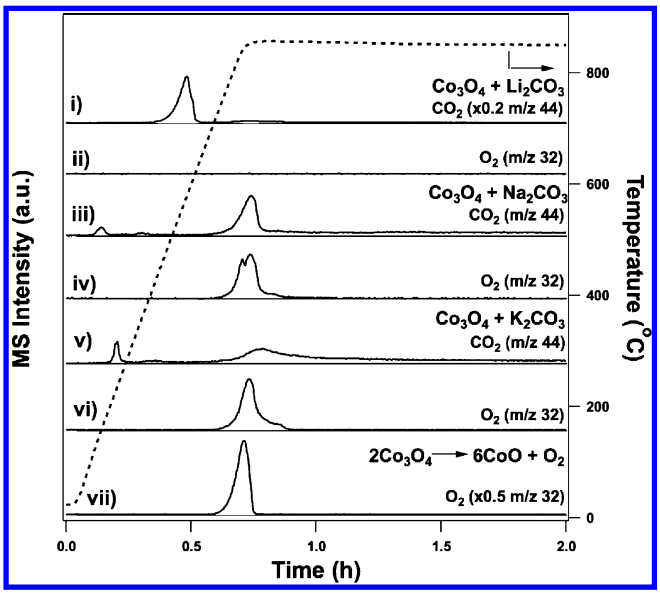

Figure 11. Reaction of Co_3O_4 with Li_2CO_3 ((i) and (ii)), Na_2CO_3 ((iii) and (iv)), and K_2CO_3 ((v) and (vi)) during the temperature ramp-and-hold procedure to 850 °C in Ar. (vii) shows the control experiment of thermal reduction of Co_3O_4 to CoO, releasing O_2.

Na_2CO_3 mixture to 850 °C, as evidenced by the powder XRD measurement and the O_2 evolution peak at ~850 °C for pure Co_3O_4.

■ DISCUSSION

Comparison of Reactivity among Alkali Carbonates. The ability of alkali carbonates to promote hydrogen evolution and CO_2 reduction with a given metal oxide that has a spinel structure follows the descending order: $Li_2CO_3 > Na_2CO_3 > K_2CO_3$ (e.g., evaluated by the onset temperatures for hydrogen evolution and CO_2 reduction reactions on various combinations of Mn_3O_4 and alkali carbonates (Table 1)). D_2 starts to evolve on Li_2CO_3/Mn_3O_4 at 540 °C, and in contrast no detectable amount of D_2 was observed on Na_2CO_3/Mn_3O_4 until 850 °C. In addition, the peak rate of D_2 evolution on Li_2CO_3/Mn_3O_4 is ~50 times that measured from Na_2CO_3/Mn_3O_4. No D_2 evolution is detected for K_2CO_3/Mn_3O_4 at reaction temperature up to 850 °C. For the CO_2 reduction reaction, the onset temperatures for CO evolution are 675, 735, and 805 °C for Li_2CO_3/Fe_3O_4, Na_2CO_3/Fe_3O_4, and K_2CO_3/Fe_3O_4, respectively, further confirming the trend in reactivity for the carbonates investigated. Reactivities of various combinations of spinel metal oxides and alkali carbonates for hydrogen evolution and CO_2 reduction reactions are summarized in Figures 13 and 14, respectively.

Hydrogen evolution @850°C	Fe_3O_4	Mn_3O_4	Co_3O_4
Li_2CO_3	✔	✔	✗
Na_2CO_3	✔	✔	✗
K_2CO_3	✔	✗	✗

Figure 13. Summary of the combinations of spinel metal oxides and alkali carbonates for hydrogen evolution reaction at 850 °C.

CO_2 reduction @850°C	Fe_3O_4	Mn_3O_4	Co_3O_4
Li_2CO_3	✔	✔	✗
Na_2CO_3	✔	✗	✗
K_2CO_3	✔	✗	✗

Figure 14. Summary of the combinations of spinel metal oxides and alkali carbonates for CO_2 reduction reaction at 850 °C.

Comparison of Reactivity among the Spinel Metal Oxides. The reactivity for hydrogen evolution and CO_2 reduction reactions of spinel metal oxides with a given alkali carbonate follows the descending order: $Fe_3O_4 > Mn_3O_4 > Co_3O_4$. Hydrogen evolution occurs on Fe_3O_4 with all three alkali carbonates, whereas Mn_3O_4 must be combined with the more reactive carbonates, that is, Li_2CO_3 and Na_2CO_3, for the evolution of hydrogen to be observed. For Co_3O_4, hydrogen evolution does not occur even when it is combined with the most reactive lithium carbonate. This reactivity trend is more pronounced for the CO_2 reduction reaction, which occurs on all Fe_3O_4 containing samples with alkali carbonates. In contrast, only when Mn_3O_4 is combined with lithium carbonate can CO

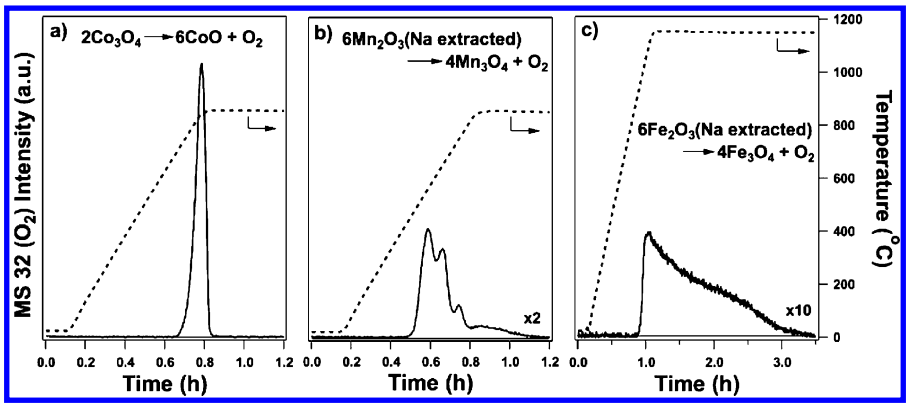

Figure 12. Thermal reduction of (a) Co_3O_4, (b) Na ion extracted Mn_2O_3, and (c) Na ion extracted Fe_2O_3.

dx.doi.org/10.1021/cm3038747 | Chem. Mater. XXXX, XXX, XXX−XXX

evolution be detected. None of the Co_3O_4 containing samples is active for CO_2 reduction at or below 850 °C.

Comparison of Ion Extraction and Thermal Reduction of Metal Oxides. The extraction of alkali cations from the alkali metal(III) oxides is key to being able to close the thermochemical cycle at reasonable temperatures (<1000 °C), since alkali metal(III) oxides cannot easily be thermally reduced (<1500 °C). The degree of difficulty for alkali cation extraction parallels the reactivity of the corresponding alkali carbonates: $Li^{\pm} > Na^{\pm} > K^{\pm}$. No appreciable lithium extraction is observed for $LiFeO_2$ and $LiMnO_2$, whereas almost complete sodium extraction can be achieved for both $NaFeO_2$ and $NaMnO_2$ (Figure 15). Furthermore, complete potassium cation removal can also be achieved by the water/CO_2 treatment from $KFeO_2$.

Alkali ion extraction @80°C (aq.)	Fe_3O_4	Mn_3O_4	Co_3O_4
Li_2CO_3	✗	✗	NA
Na_2CO_3	✔	✔	NA
K_2CO_3	✔	NA	NA

Figure 15. Summary of alkali ion extraction from the alkali metal salts formed in the hydrogen evolution reaction in an aqueous suspension at 80 °C in the presence of CO_2.

Tuning the Operating Temperature of Thermochemical Cycles. A general trade-off exists between the temperatures of oxidation (M(II) → M(III)) and reduction (M(III) → M(II)) reactions of the metal species in the thermochemical cycle presented in this work: the lower the reaction temperature in one direction is generally compensated by a higher reaction temperature in the other direction. For example, hydrogen evolution temperatures for Fe_3O_4-based cycles are lower than those of Mn_3O_4-based cycles (Table 1); whereas the complete thermal reduction of Fe_2O_3 to Fe_3O_4 (~1150 °C) occurs at higher temperature than that of Mn_2O_3 to Mn_3O_4 (~850 °C) (Figure 12). The range of heat sources a specific thermochemical cycle can take advantage of is often limited by the step with the highest operating temperature. Therefore, metal oxides with balanced redox properties, that is, with hydrogen evolution and thermal reduction reactions occurring at similar temperatures, lead to low overall operating temperature. The Mn_3O_4-based thermochemical cycle falls in that category, as the hydrogen evolution and thermal reduction reactions both occur at ~850 °C.

CONCLUSIONS

Low-temperature thermochemical cycles for water splitting and CO_2 reduction involving spinel metal oxides and alkali carbonates were investigated. The reactivity sequence for hydrogen evolution reaction of metal oxides with a given alkali carbonate is $Fe_3O_4 > Mn_3O_4 > Co_3O_4$; whereas that of alkali carbonates with a given metal oxide is $Li_2CO_3 > Na_2CO_3 > K_2CO_3$. Hydrogen evolution and CO_2 reduction reactions occur at lower temperature on the more reactive combinations of metal oxide and alkali carbonate; however, thermal reduction temperature is higher and the alkali ion extraction is more difficult for the more active metal oxide and alkali carbonate, respectively. Mn_3O_4/Na_2CO_3 appears to be the best combination in that the temperatures required for hydrogen evolution and thermal reduction of metal oxide are similar. In addition, complete alkali ion extraction can be achieved for the Mn_3O_4/Na_2CO_3 combination.

ASSOCIATED CONTENT

Supporting Information

Further details are given in Figure S1. This material is available free of charge via the Internet at http://pubs.acs.org.

AUTHOR INFORMATION

Corresponding Author

*E-mail: mdavis@cheme.caltech.edu.

Notes

The authors declare no competing financial interest.

ACKNOWLEDGMENTS

Financial support of this work was provided by a donation from Mr. and Mrs. Lewis W. van Amerongen. The authors would like to thank Dr. J. Labinger for helpful discussions of this work.

REFERENCES

(1) Kehlhofer, R.; Rukes, B.; Hannemann, F.; Stirnimann, F. *Combined-Cycle Gas & Steam Turbine Power Plants*; PennWell Books: Tulsa, OK, 2009.
(2) Abanades, S.; Legal, A.; Cordier, A.; Peraudeau, G.; Flamant, G.; Julbe, A. *J. Mater. Sci.* **2010**, *45*, 4163−4173.
(3) Chueh, W. C.; Falter, C.; Abbott, M.; Scipio, D.; Furler, P.; Haile, S. M.; Steinfeld, A. *Science* **2010**, *330*, 1797−1801.
(4) Rosen, M. A. *Energy* **2010**, *35*, 1068−1076.
(5) Forsberg, C. *Prog. Nucl. Energy* **2005**, *47*, 32−43.
(6) Brown, L. C.; Besenbruch, G. E.; Schultz, K. R.; Marshall, A. C.; Showalter, S. K.; Pickard, P. S.; Funk, J. F. In *Proceedings of the International Congress on Advances in Nuclear Power Plants*; 2002
(7) Xu, B.; Bhawe, Y.; Davis, M. E. *Proc. Natl. Acad. Sci. U.S.A.* **2012**, *109*, 9260−9264.
(8) Meredig, B.; Wolverton, C. *Phys. Rev. B* **2009**, *80*, 245119.
(9) Kreider, P.; Funke, H.; Cuche, K.; Schmidt, M.; Weimer, A. W. *Int. J. Hydrogen Energy* **2011**, *36*, 7028−7037.
(10) Francis, T.; Lichty, P.; Weimer, A. W. *Chem. Eng. Sci.* **2010**, *65*, 3709−3717.
(11) Sturzenegger, M.; Ganz, J.; Nüesch, P.; Schelling, T. *J. Phys. IV France* **1999**, *09*, Pr3−331−Pr3−335.
(12) Sturzenegger, M.; Nüesch, P. *Energy* **1999**, *24*, 959−970.
(13) Kaneko, H.; Hosokawa, Y.; Gokon, N.; Kojima, N.; Hasegawa, N.; Kitamura, M.; Tamaura, Y. *J. Phys. Chem. Solids* **2001**, *62*, 1341−1347.
(14) Xu, B.; Madix, R. J.; Friend, C. M. *J. Am. Chem. Soc.* **2010**, *132*, 16571−16580.